Direct oxidation of methane to methanol on Co embedded N-doped graphene: Comparing the role of N_2O and O_2 as oxidants

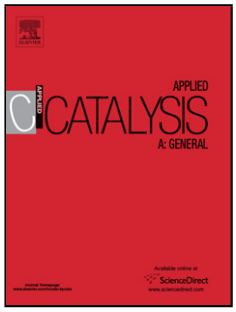

Direct oxidation of methane to methanol on Co embedded N-doped graphene: comparing the role of N_2O and O_2 as oxidants

Parisa Nematollahi, Erik C. Neyts

PII: S0926-860X(20)30309-4

DOI: https://doi.org/10.1016/j.apcata.2020.117716

Reference: APCATA 117716

To appear in: *Applied Catalysis A, General*

Received Date: 17 December 2019

Revised Date: 19 June 2020

Accepted Date: 22 June 2020

Please cite this article as: Nematollahi P, Neyts EC, Direct oxidation of methane to methanol on Co embedded N-doped graphene: comparing the role of N_2O and O_2 as oxidants, *Applied Catalysis A, General* (2020), doi: https://doi.org/10.1016/j.apcata.2020.117716

Direct oxidation of methane to methanol on Co embedded N-doped graphene: comparing the role of N_2O and O_2 as oxidants

Parisa Nematollahi*[a] and Erik C. Neyts[a]

[a] Research Group Plasmant, NANOlab Center of Excellence, Department of Chemistry, University of Antwerp, Universiteitsplein 1, 2610 Antwerp, Belgium

*Corresponding author. **Phone:** (+32) 32652346. **E-mail**: parisa.nematollahi@uantwerpen.be

Graphical abstract

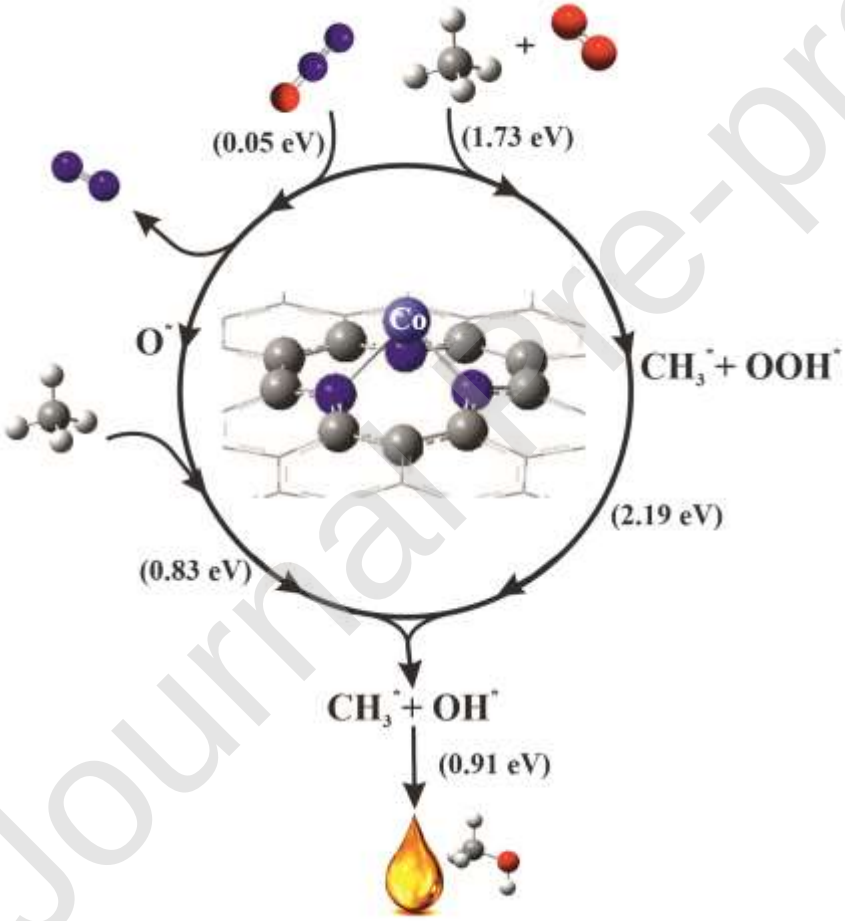

Highlights

- The CoN_3–G shows better catalytic activity toward adsorption of gas reactants and consequently methane oxidation.
- Methane converts to methanol on CoN_3-G via a two-step pathway, employing N_2O as an oxygen- donor.
- The C-H bond cleavage proceeds via the Eley-Rideal (ER) mechanism while other reactions proceed via the Langmuir-Hinshelwood (LH) mechanism.
- Methane dissociates actively on CoN_3-G results in the formation of ethane molecule in a C-C coupling reaction during the oxidation process.

Abstract

In this work, the effects of N-doping into the Co-doped single vacancy (Co-SV-G) and di-vacancy graphene flake (Co-dV-G) are investigated and compared toward direct oxidation of methane to methanol (DOMM) employing two different oxidants (N_2O and O_2) using density functional theory (DFT) calculation. We found that DOMM on CoN_3-G utilizing the N_2O molecule as oxygen-donor proceeds via a two-step reaction with low activation energies. In addition, we found that although CoN_3-G might be a good catalyst for methane conversion, it can also catalyze the oxidation of methanol to CO_2 and H_2O due to the required low activation barriers. Moreover, the adsorption behaviors of CH_x (x=0-4) species and dehydrogenation of CH_x (x=1-4) species on CoN_3-G are investigated. We concluded that CoN_3-G can be used as an efficient catalyst for DOMM and N_2O reduction at ambient conditions which may serve as a guide for fabricating effective C/N catalysts in energy-related devices.

Keywords: N-doped graphene, direct oxidation of methane, DFT, methanol, N_2O reduction, Co embedded grapheme

1 Introduction

Traditional conversion of methane (CH_4) to methanol (CH_3OH) is performed by a two-step process in the industry under the harsh reaction conditions such as high temperature and pressure [1, 2]. Despite the fact that it is not a cost-effective procedure, there exists no industrial process capable of directly converting methane to methanol. In addition, N_2O is known as an agricultural toxic gas which may also originate from other activities like wastewater treatments, or the combustion of fossil fuels and biomass. During the last century, it is found that the global warming of CH_4 and N_2O are 28 and 265 times higher than CO_2. Therefore, investigating the conversion of these gas molecules is of great interest. Direct synthesis of CH_3OH from CH_4 at room temperature and pressure is a promising way for the industry. To date, many studies have been explored on the direct synthesis of methanol but none of them has proven cost-effective. Thus, it remains one of the considerable challenges in the sector of methane utilization due to the strong C–H bond energy and its chemical inertness of methane.

It is known that although noble metals like Ir, Pt, Rh and Ru [3-7] are highly active toward DRM and resistant to carbon formation, they are economically less attractive materials for large-scale industrial use due to their scarcity, high cost and toxicity [8]. Amongst different types of catalysts, single individual metal atoms anchored to graphene-based materials [9-11] are discovered as novel material not only because they minimize material usage to meet the goal of cost-effective catalysis, but also because they surpass conventional catalysts in terms of having a high specific activity with a significantly reduced amount of noble metals. Recently, single metal atoms doped into monolayer surfaces have been tested as catalysts for various reactions owing to their well-defined sites, unsaturated coordination environment, and high atom efficiency. Doping single-atoms into the graphene structure may be effective to improve its catalytic properties [12, 13]. Amongst an increasing number of single-atoms, most have been focusing on supporting noble metal atoms like Pt or Pd on metal oxide or metal surfaces [14, 15]. Dopants such as P [16], Si [17, 18], Fe [19, 20], Pt [21, 22], Pd [23, 24], Ni [25, 26] substitute with carbon atoms in the graphene sheet and can significantly enhance the properties of graphene sheet. On the other hands, tailoring the graphene sheet by introducing defects [27, 28] or heteroatoms (e.g., N, B, P) [29] into the structure of graphene sheet will speed up the catalytic reactions occurred on the surface [30, 31] and modulate the electronic properties of the catalyst [32-35].

It has been reported that N-doped graphene (N-G) [36] and transition metal-coordinated nitrogen-doped graphene (TMN-G) can enhance the chemical reactivity of graphene due to their low cost, high durability, and high catalytic activity. They are widely used in molecular sensors [37, 38], bio-sensing applications [39], metal-free oxygen reduction catalysis (ORR) [40, 41], CO oxidation reactions [42], and in lithium batteries [43-45]. The introduced N atoms modify the energy distribution of electronic states and thereby the local reactivity [46]. Three common N-doped configurations are observed in N-G, i. e., pyridinic, pyrrolic, and graphitic nitrogen [47, 48]. However, there are no investigations toward the differences of catalytic ability between different N defects. Recently, it was found that pyridinic-N can better anchor transition metal atoms in comparison to other types of N-G, due to their higher stability and catalytic activity toward various reactions [49, 50]. For instance, Yeager et al. [51] found that metal cations coordinated by pyridinic nitrogen-doped at the defective sites of graphitic carbon are the active sites for ORR in alkaline and acid electrolytes. Experimentally, graphene or carbonic structures containing nitrogen-coordinated transition metals can be easily synthesized [33, 52, 53]. Recently, Fei et al. [54] worked on the synthesis of nitrogen-enriched core-shell structured cobalt-carbon nanoparticles dispersed on graphene sheets, which can be used for hydrogen evolution reaction in both acidic and basic media. Wang et al. [55] found that Co embedded N-doped carbon nanotubes have high activity toward ORR and the oxygen evolution reaction (OER) in both alkaline and neutral

media due to their low cost and appropriate features to act as bifunctional catalysts for both the ORR and OER.

In the last few decades, researchers have been dedicated to the synthesis of cost-effective electrocatalysts using cheaper transition metals [56] in which, cobalt-based electrocatalysts show the most promising results [57]. As of any first-row transition metal (Ni, Fe, and Cu), cobalt is a cheap, environmentally friendly, and accessible metal in comparison with noble metals [58] and it can be introduced into the graphene lattice with no difficulties [10]. Recently, Fei et al. [54] worked on the synthesis of nitrogen-enriched core-shell structured cobalt-carbon nanoparticles dispersed on graphene sheets, which can be used for hydrogen evolution reaction in both acidic and basic media. In an experimental investigation, Jurković et al. [59] reported the plasma- activated methane partial oxidation reaction in a designed dielectric barrier discharge ionization reactor unit. They could produce valuable platform chemicals like methanol, formaldehyde, intermediate formic acid, acetic acid, and paraformaldehyde at room temperature and atmospheric pressure. Moreover, it is found that Co nanoparticles doped into carbon nanotube structures can decrease the local work function of the carbon surface because electrons transfer from cobalt to the surrounding carbon atoms, very easily [60]. Kattel et al. [61] investigated the ORR reaction pathway on M–N (M = Fe, Co, or Ni) catalytic clusters formed between pores in graphene supports. They found that O_2 molecule chemisorbs on CoN_4-graphene (CoN_4-G) and FeN_4-graphene (FeN_4-G) clusters but not on NiN_4-graphene (NiN_4-G) clusters. Therefore, the first two clusters were regarded as more active substrates toward ORR. The high stability is mainly attributed to the high conductivity of N-doped graphene and the embedded Co nanoparticles. N-doping increases the electron donor-acceptor properties of graphene and leads to the improvement of the conductance and interfacial electron transfer by doped Co nanoparticles [62]. Zhang et al. [49] calculated the activation barriers and thermodynamic properties of ORR on CoN_4-G. They demonstrated that CoN_4-G can enhance the ORR and resulted in the formation of two H_2O molecules. Kiefer et al. [63] reported that graphitic CoN_4 defects are stable at all potentials (U = 0-1.23 V) while CoN_2 defects are predicted to be unstable at high potentials. In addition, they predicted that the CoN_4 defect is the dominant in-plane graphitic defect in CoN_x/C electrocatalysts.

Graphene nano-flakes and graphene nano-ribbons are promising graphene-based materials with a size controllable energy bandgap, which might be useful for various technological applications [64, 65]. They are important because of their potential for bottom-up fabrication of molecular devices, spintronic, and quantum dot technology [66]. They are cheap catalysts and being produced by a cheap method, they typically contain many defects. Because of the small size of graphene flakes they can be considered as a zero-dimensional form of graphene sheet showing different properties from graphene nanoribbons and bulk graphene. Such graphene-flakes are promising for a variety of applications such as electronic and magnetic devices with different molecular sizes and shapes, and in light absorption in photovoltaics due to their edge structure and wide spectrum. They have unique electronic, magnetic, and optical properties since their bandgap can be modified. Moreover, the saturation of the zigzag edges of graphene flakes with different atoms (like H in our investigations) or molecular groups leads to a spin-polarized ground state with a non-zero total magnetic moment, an electronic energy gap, and spin density that strongly depends on the used atomic group to passivate the dangling bonds of the C atoms [67]. In this study, we have chosen to model such a graphene flake as a polyaromatic hydrocarbon molecule (PAH).

This article describes our efforts to develop a mechanism for methane conversion to methanol on a modified graphene flake. The modification of the graphene flake has been done in three steps, i. e., introducing a single vacancy (SV) and di-vacancy (dV) defect, doping the defective flake with nitrogen heteroatoms making pyridinic N-doping graphene flake (N_3- and N_4-G), and finally

introducing a single Co atom into the defective graphene flake lattice. Then, we investigated and compared the effect of nitrogen doping on the catalytic activity of the designed catalysts toward direct oxidation of CH_4 to CH_3OH using O_2 and N_2O as an oxidant. N_2O acts as an O-donor compound and gives us the ability to convert two pollutant gas simultaneously. The effects of using different oxidants have been studied in several investigations. For instance, Dasireddy et al. [68] studied the effects of oxidants (H_2O, N_2O, and O_2) on methane oxidation to methanol over the $FePO_4$ catalyst. They found that $FePO_4$ can actively convert methane to methanol using O_2 and N_2O oxidants.

It should be noted that although Ni or Cu metal surfaces would be most effective for C-H bond cleavage, the activity of an individual single Ni or Cu atoms doped graphene-like surfaces will vary toward the same reaction. For instance, in our previous investigation [69], single Ni and Si atoms were chosen to compare the catalytic activity of the tuned graphene flake toward the direct conversion of methane to methanol. Interestingly, we found that single Ni atom doped graphene flake (Ni-G) cannot actively catalyze methane oxidation while Si-doped graphene flakes (Si-G) showed a better catalytic activity thanks to the lower activation energies and more favourable thermodynamic properties. Therefore, we reasonably assume that depending on the investigated graphene nano-flake (with applying different tuning methods), the activity of an arbitrary doped single metal atom and consequently the whole tailored graphene nano-flake will change. Motivated by previous investigations, in this article, a single Co atom is chosen as a single metal atom due to its considerable activity for ORR and OER. Density functional theory (DFT) calculations are utilized in order to find the most energetically favourable substrate for the direct oxidation of methane to methanol. All the reactions take place at room temperature and then the catalytic performances of these carbon material catalysts were investigated. Moreover, the detailed surface interactions and reaction pathways that occurred on the interface of the substrate were also discussed.

2 Computational details

All structure optimizations and reaction pathway calculations are based on DFT using the Gaussian 16 package [70]. We employed the meta-GGA hybrid functional M06-2X [71] for geometry optimizations and frequency calculations. For carbon, nitrogen, hydrogen, and oxygen atoms the all-electron 6-31G* basis set is used. The Los Alamos National Laboratory [72] basis set of double-ξ quality (LANL2DZ) used for Co atom. No significant spin contamination was found. To model the pristine graphene as a finite-size monolayer flake, a total of 85 carbon atoms were considered for all calculations. To minimize the boundary effect by dangling bonds, the edge atoms of the graphene flake are saturated by hydrogen. The binding/adsorption energy (E_{ads}) of each of the gas species involved in the reaction mechanism is characterized as:

$$E_{(bind/ads)} = E_{(AB)} - E_{(A)} - E_{(B)} \quad (1)$$

It is defined as the difference between the total energy of the optimized adsorbate-substrate system, $E_{(AB)}$, the sum of the total energy of the pure substrate, $E_{(A)}$, and the total energy of the optimized adsorbates or single metal atom in the gas phase, $E_{(B)}$. Moreover, the triplet state oxygen is considered for the adsorption configurations. The zero-point energy (ZPE) correction to the energy of adsorbed molecular species was calculated by:

$$ZPE = \sum_i \frac{1}{2} h\vartheta_i \quad (2)$$

where h and ϑ_i are Planck's constant and the frequency of the i^{th} vibrational mode, respectively. Natural bond orbital (NBO) analysis is used to measure the overlap population between two atoms. The formation energies (E_f) of Co-doped N embedded graphene flake are calculated by:

$$E_f = E_{substrate} + a\mu_C - (E_{pureG} + b\mu_N + \mu_{Co}) \quad (3)$$

the $E_{substrate}$ represents the total energy of the doped graphene flake, μ_C and μ_N are the chemical potentials of the carbon and nitrogen atom, defined as the total energy per carbon atom in a pure graphene flake and the one-half of gaseous N_2 molecule, respectively. a (b) coefficients for CoN_3-G and CoN_4-G are 4(3) and 6(4), respectively. Finally, μ_{Co} is the energy for isolated Co atom. Frontier Molecular Orbitals consist of the highest occupied molecular orbital (HOMO) and the lowest unoccupied molecular orbital (LUMO), which play an important role in the chemical reactivity of the molecule. The location of the HOMO determines the ability of electron donation while the LUMO dictates the ability to accept an electron. The molecular orbital calculations were also performed for all adsorbents at the same level of theory. The electronic properties of the substrates were calculated using Multiwfn 3.3.9 [73]. Additionally, electron density difference [74] (EDD, $\Delta\rho$) for the adsorbed structures are also studied to understand the interaction between the substrate and adsorbate. It is defined as:

$$\Delta\rho = \rho_C - \rho_A - \rho_S \quad (4)$$

where the ρ_C, ρ_A, and ρ_S are the electron charge densities of the adsorbed species on the substrate system, the free adsorbate, and the pristine graphene flake, respectively. In the EDD maps, the charge depletion and charge accumulation areas denoting as blue and red colors, respectively.

The thermodynamic properties of the reactions are calculated from the frequency calculations according to the following equations [75]:

$$\Delta H = \sum (\varepsilon_0 + H_{corr})_{\text{products}} - \sum (\varepsilon_0 + H_{corr})_{\text{reactants}} \quad (5)$$

$$\Delta G = \sum (\varepsilon_0 + G_{corr})_{\text{products}} - \sum (\varepsilon_0 + G_{corr})_{\text{reactants}} \quad (6)$$

$$H_{corr} = E_{tot} + k_B T \quad (7)$$

$$G_{corr} = H_{corr} - TS_{tot} \quad (8)$$

where ε_0 is the total electronic energy at T = 0 K and k_B is the Boltzmann constant. The internal thermal energy E_{tot} is obtained from translational (E_{tr}), rotational (E_{rot}), vibrational (E_{vib}), and electronic (E_{el}) energies, and S_{tot}, S_{tr}, S_{rot}, S_{vib}, S_{el} are the corresponding entropies. H_{corr} and G_{corr} refer to thermal corrections which should be added to ε_0 to obtain the enthalpy and Gibbs free energy, respectively. For all the reactions, the transition state (TS) located by analytical methods as defined in the default Gaussian 16 method. Vibrational frequency calculations performed for all the TS structures at the DFT-optimized geometries with the default Gaussian 16 algorithm having only one negative imaginary frequency. To characterize the nature of all transition state structures, the existence of the corresponding imaginary frequency along with intrinsic reaction coordinate (IRC) calculations was considered [76]. Reaction paths were followed for the ground state spin of the states for each reaction.

According to the NIST database, the oxidation of methane to methanol $2CH_{4\,(g)} + O_{2\,(g)} \rightarrow 2CH_3OH_{(g)}$ is a thermodynamically favourable reaction, $\Delta G^{\circ}_{298.15}$ = -2.32 eV and $\Delta H^{\circ}_{298.15}$ = -2.63 eV. The calculated thermodynamic results for this reaction using Gaussian16 also declare that it is a thermodynamically feasible reaction. $\Delta G_{298.15}$ = -1.87 eV and $\Delta H_{298.15}$ = -2.20 eV, in order to diminish or reduce the existed difference between the calculated thermodynamic values by Gaussian and those we obtained from the NIST database, we investigated the thermodynamic properties of the reaction by applying various functional and basis sets. The obtained results are provided in Table S3. The best agreement with the NIST database data was found using the CBS-QB3 functional [77] with 6-311G** basis set, viz. ΔG = -2.35 eV and ΔH = -2.66 eV, which is indeed very close to the database values.

3 Results and discussion

This work aims to investigate the catalytic activity of Co-SV-G, Co-dV-G, CoN_3-G, and CoN_4-G toward methane activation and conversion to methanol using N_2O and O_2 as an oxidant. In most cases, the methane oxidation reaction starts with C-H bond cleavage that is a challenge in heterogeneous catalysis, because of its great thermodynamic stability (435 kJ mol^{-1}) and strong tetrahedral bonds. Therefore, upon C-H bond cleavage, two different pathways with different intermediates can be identified for the H abstraction by oxygen: a radical and a non-radical process [78]. The possibility of the reaction to proceed via the Eley-Rideal (ER) and Langmuir-Hinshelwood (LH) mechanism is also investigated in detail.

3.1 Geometric and electronic properties of the substrates

Since the stability of doped graphene determines its usage in catalysis applications, an evaluation of the surface stability is required. The studied substrates are produced in three steps: (I) the creation of single vacancy graphene flake (SV-G) by removing one carbon atom (see Figure 1, labeled X)), and divacancy graphene flake (dV-G) by removing two carbon atoms, (labeled C3 and X)); (II) the replacement of three and four undercoordinated C atoms with N atoms to form the defective N_3-G and N_4-G, respectively; (III) incorporation of Co atom in the center of the SV-G, dV-G, N_3-G and N_4-G making Co-SV-G, Co-dV-G, CoN_3-G, and CoN_4-G, respectively. These substitutions were employed in similar theoretical studies [79-81]. Figure 1 shows the optimized configurations of each substrate. NBO charge analysis (q) of each substrate along with the calculated binding energy of Co atom into the vacancy sites, E_f, energy gap (E_g), and the corresponding thermodynamic properties are listed in Table 1.

For pure graphene, we find a C-C bond length of 1.42 Å that is similar to the experimental value [82]. Working with a graphene flake, a bandgap is expected. We calculate an energy gap of E_g = 2.66 eV, which is used as a reference for comparing the geometry and electronic properties of doped configurations (see Table 1). These values are in good agreement with other theoretical and experimental studies [83-85]. In the graphene flake, a single carbon atom adsorbs with an adsorption energy of -7.23 eV into the single vacancy of graphene. One can see that in the SV-G, a five and nine-member ring (5-MR and 9-MR) are produced with C1-C2, C1-C3, and C2-C3 bond lengths of 1.76, 2.77, and 2.81 Å, respectively. By introducing a single Co atom into the SV-G configuration, the Co atom covalently binds to three surrounding carbon atoms of the vacancy site with equal Co-C bond lengths of 1.78 Å. These values are also in good agreement with previous studies (Co-C=1.79-1.90 Å) [86, 87]. Due to the larger atomic radius, the Co atom is pushed outward from the graphene plane in a tetrahedral-like configuration with respect to the neighbouring C atoms (see Figure 1), at a height of 1.29 Å above the graphene flake. This result is also in good agreement with other doped metal atoms into the graphene sheet [88, 89]. The calculated binding energy of the single Co atom into the SV-G is E_{bind}= -4.52 eV. To compare charge distributions in the Co-G structures, NBO charges are calculated for all obtained structures. In Co-G, a small charge of +0.25 e is transferred from the Co atom to the surrounding carbon atoms of the vacancy site making the neighbouring carbon atoms negatively charged (-0.30 e) with Co-C bonds of 1.78 Å.

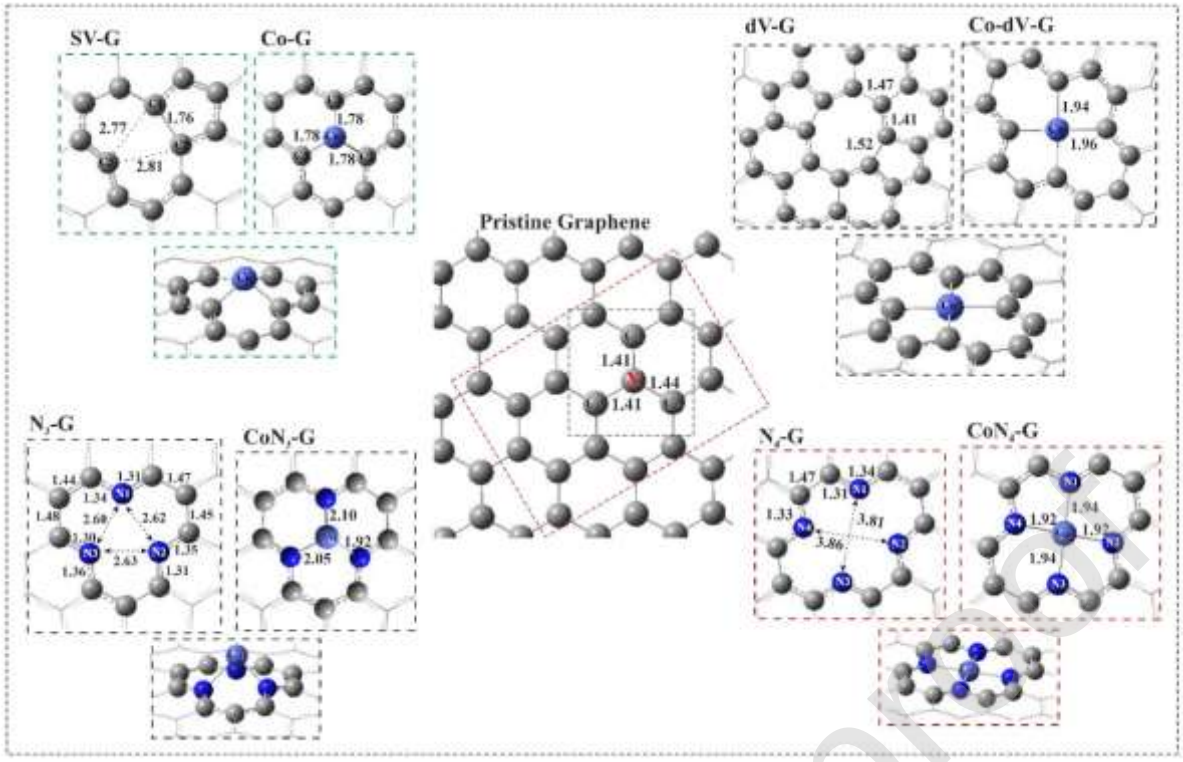

Figure 1. The geometric structure of pristine graphene flake, Co-SV-G, Co-dV-G, CoN_3-G, and CoN_4-G. All bond lengths are in Å.

In the dV-G, first, a 5-8-5 defect [90] is produced and then by introducing the Co atom into the vacancy site, Co-dV-G forms (see Figure 1) with low binding energy of E_{bind}= -1.90 eV. According to the NBO charge analysis, a charge of +0.65 e is transferred from the Co atom to the surrounding C atoms of the vacancy site leading to negatively charged C atoms (-0.85 e) with Co-C bond lengths of Co-C = 1.96 Å. If three or four surrounding C atoms of the SV-G or dV-G are substituted by three or four nitrogen atoms, a defective pyridinic N_3-G or N_4-G is created, respectively. According to the previous studies, the presence of pyridinic-N atoms around any defect sites might affect the electronic structure of graphene [89, 91]. The substitution of the vacancy C atoms by N atoms can considerably reduce the formation energy of the mono- or di-vacancy graphene sheet. The reason may refer to the vanishing of the existed dangling bonds in these systems. So, it is clear that the N embedded graphene structures are the dominant configurations. According to the NBO charge analysis, each nitrogen atom in N_3-G and N_4-G is negatively charged to -0.5 e showing that these negative sites are active enough to trap the Co atom making the CoN_3-G and CoN_4-G.

Table 1. The calculated NBO analysis (+ and – signs refer to the electron donation and acceptation), binding energy (E_{bind}), formation energy (E_f), energy gap (E_g), change of enthalpy (ΔH_{298}), and change of Gibbs free energy (ΔG_{298}) of pure graphene flake, Co-SV-G, Co-dV-G, CoN_3-G and CoN_4-G.

Complex	$q_{(Co/C\ or\ N)}$(e)	E_{bind} (eV)	E_f (eV)	E_g (eV)	$\Delta H_{298.15}$(eV)	$\Delta G_{298.15}$(eV)
graphene	+0.04	-7.23	-	2.66	-7.19	-7.23
Co-SV-G	+0.25 (-0.30)	-4.52	2.71	3.06	-4.47	-4.18
Co-dV-G	+0.65 (-0.85)	-1.90	3.31	1.78	-1.91	-1.65
CoN_3-G	+0.46 (-1.86)	-4.58	-0.95	2.48	-4.53	-4.21
CoN_4-G	+0.74 (-2.80)	-7.81	-3.47	3.20	-7.67	-7.28

In CoN_3-G, the Co atom and the surrounding three nitrogen atoms of the vacancy site are positively

(0.46 e) and negatively (-1.86 e) charged, respectively. Therefore, the CoN_3 moiety is negatively charged by -1.4 e with the formation energy of E_f = -0.95 eV. Upon adsorption of a single Co atom into the defective N_3-G, the average bond length of Co-N is increased considerably to 2.02 Å, pushing the Co atom of the basal plane by 1.36 Å from the graphene flake surface. The calculated binding energy of Co on the N_3-G is E_{bind} = -4.58 eV, which is higher than that of PdN_3-G (E_{bind} = -3.19 eV) [92] and is quite close to that reported by Zhang et al. (E_{bind} = -4.84 eV) [93].

In the defective N_4-G, Co-N2/N4 and Co-N1/N3 bond lengths are equal to 1.92 Å and 1.94 Å, respectively, in agreement with Orellana et al. study (Co-N =1.90 Å) [81]. In contrast to CoN_3-G, the Co adatom adsorbs in the pyridinic N_4-G and lies in the plane format by nitrogen atoms with the formation energy of E_f = -3.47 eV. The higher formation energy of CoN_4-G than CoN_3-G indicates that the Co atom can be more easily interact with the nitrogen atoms of the di-vacancy site than those in the single vacancy site. It adsorbs strongly into the N_4-G site with E_{bind} = -7.81 eV. The high adsorption energy can be related to the additional valence electrons available from the substitutional N atoms that stabilize the unpaired electron of the coordinated C atom of the graphene flake. This results in a higher charge transfer (≈ 0.74 e) from the Co atom to the four nearest N atoms of the surface, which are all negatively charged by ≈ -2.8 e. Also, it is consistent with the high electronegativity of nitrogen atoms compared with that of carbon and Co atoms, such that the Co atom binds stronger with its neighbouring N and C atoms than those in CoN_3-G and Co-G, respectively.

The EDD of three stable substrates is shown in Figure S1 in the Supporting information. In Co-G, the charge is mostly accumulating on the surrounding C atoms while we found that the transferred electrons from Co atom and three neighbouring N atoms induce the charge redistribution at their interfaces. Also, as shown in Figure S1, the charges mainly accumulate on the N atoms illustrating that more electrons (>1.0 e) are transferred from Co dopant to the neighbouring N atoms leading to the enhancement of their interaction. Similar to CoN_3-G, in CoN_4-G the transferred charge from the Co atom to the four adjacent N atoms is high, and electrons dominantly accumulate on N atoms and around the Co-N bonds. These results indicate that the N_4-G could efficiently stabilize the embedded Co atom, which is stable enough to be used in the catalytic reactions.

Furthermore, by inspecting the electronic states of CoN_3-G and CoN_4-G near the Fermi level we can better understand the reason for having such large adsorption energies. One can see from Figure S2 that there are strong electron coupling between the 3d orbitals of Co atom and the 2p orbitals of N atoms around the Fermi level confirming the existence of covalent Co-N bond in the studied substrates. By doping Co atom into the vacancy site, Co atom pulls down the unoccupied localized anti-bonding states of N atoms to near the Fermi level indicating that when Co atom adsorbs over the vacancy sites, those states are partially occupied. In addition, the incorporation of N atoms shifts the bandgap above the Fermi level gradually confirming the enhancement of electron (donor) concentration states. Similar electronic results are given by Li et al. [94] reporting that the pyridinic nitrogen act as an active catalyst toward ORR [95].

Finally, we evaluate the diffusion of Co atom to its nearest vacancy site in CoN_3-G and CoN_4-G. The stable configuration of CoN_3-G and CoN_4-G is chosen as the initial state (IS). The energy profile and the related stationary structures are depicted in Figure S3. Very high diffusion barriers required to diffuse the Co atom to the nearest hollow sites of the surface in both substrates. This confirms the Co atom is stable enough at the defective N_3-G and N_4-G sites that prevents the metal clustering problem. These results are in agreement with the experimental investigations indicating that the bonded Co atom cannot be easily migrated to other hollow sites of the nitrogen-doped graphene surface through the leaching process [96].

3.2 Adsorption of gas reactants on CoN_3-G and CoN_4-G

The accumulated charge on the active Co site increases the interaction of the substrate with the gas species by increasing the polarization of the gas molecule. This was also considered in recent studies for hydrogen storage purposes [97]. There are three different active sites on each substrate, Co, N, and C. Depending on which active site the gas reactant (CH_4, O_2, N_2O) adsorbs on, different adsorption configurations will be obtained. It should be noted that for each adsorbate various adsorption sites and different adsorption patterns (including side-on and end-on) are considered. Similar to earlier reports we found that each species tends to directly interact with the metal atom at the center of the vacancy site [81, 98, 99]. The corresponding geometric structures of adsorbed gas reactants on CoN_3-G, and CoN_4-G along with their EDD maps are shown in Figure 2. Additionally, the calculated E_{ads}, NBO charge analysis, and thermodynamic properties of the species are reported in Table 2.

Various spin multiplicities were considered for each configuration, i., e. singlet, doublet, triplet, and quadruplet. Our results reveal that as a function of progress of the reaction, the spin multiplicity changes either from singlet to triplet or from doublet to quadruplet, and vice versa. The dominant spin multiplicity of some species like OH, CH_3, CH_2, CH, O, O_2, and CH_4 on Co-N_3G and CoN_4-G is different. Therefore, the energetically more stable configurations are chosen for our calculations. In addition, the adsorption behaviour of CoN_3-G and CoN_4-G toward adsorption of the gas reactants and intermediates in different spin multiplicities were also been tested. For instance, investigating the O_2 dissociation on CoN_3-G considering singlet and triplet states, we chose the triplet multiplicity for the dissociation pathway not only because the configurations are energetically more stable but also because the calculated activation barrier is lower in the triplet state (2.76 eV) than in the singlet state (3.02 eV). A similar comparison was made for other configurations. Here, the energetically more favourable structures are reported.

One can see from Figure 2 that in complexes A and D, methane molecule adsorbs physically over the Co atom, at a distance of 2.46 Å and 3.00 Å and with an adsorption energy of E_{ads} = -0.38 eV and E_{ads} = -0.21 eV, respectively. The corresponding calculated charge transfer from methane to the surface in complexes A and D is 0.14 e and 0.07 e, respectively. These weak interactions are also apparent from their EDD map, showing almost no charge accumulation around the Co-C bond in the two complexes. Interestingly, adsorption of methane on CoN_3-G is exothermic while its adsorption on CoN_4-G is not spontaneous at room temperature (see Table 2).

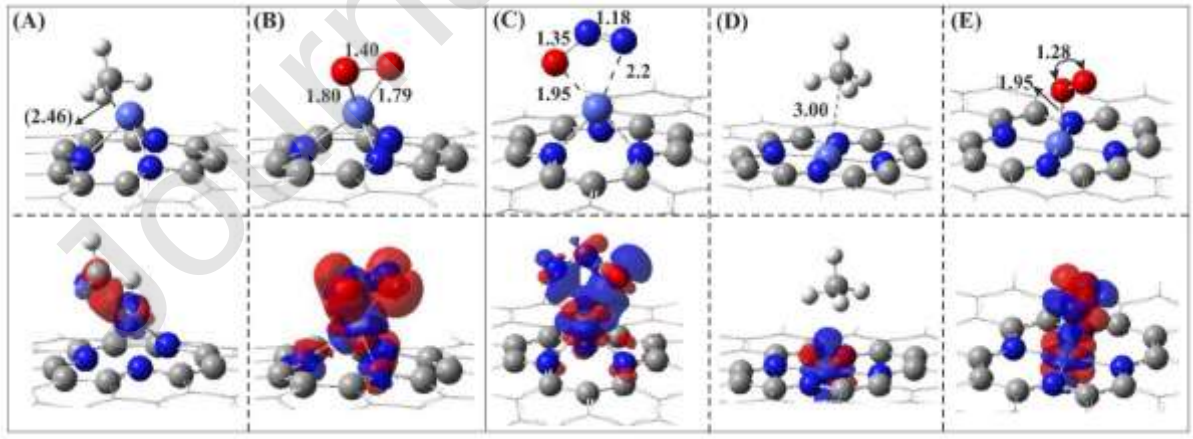

Figure 2. The most plausible geometric structures of the gas reactants on CoN_3-G and CoN_4-G along with the corresponding EDD map. All distances are in Å.

In contrast to methane, the adsorption of O_2 on CoN_3-G is quite strong. In both complexes, the O_2

molecule tends to adopt a parallel position with the surface on the Co atom. In complex B, O_2 adsorbs on the Co atom makes a V shape with two Co-O bond length of 1.80 Å and large adsorption energy of E_{ads} = -1.24 eV, which is lower than that on PtN_3-G (-1.89 eV) [100]. A charge of -0.46 e is transferred from the CoN_3-G to the adsorbed O_2 molecule which makes the Co atom more positive (+0.71 e), leading to the stronger adsorption of O_2 on the CoN_3-G surface and significant elongation of the O-O bond (1.40 Å). The EDD map of complex B correspondingly illustrates that the charge accumulation regions are mostly localized between the Co-O and O-O bonds. Furthermore, the higher reaction enthalpy for the formation of complex B shows that this substrate is more activated toward adsorption of O_2 molecule, $\Delta H_{298.15}$ = -1.22 eV, and $\Delta G_{298.15}$ = -0.72 eV.

Table 2. The calculated adsorption energy (E_{ads}), NBO charge analysis (q) (+ and – signs refer to the electron donation and acceptation), change of enthalpy ($\Delta H_{298.15}$), and change of Gibbs free energy ($\Delta G_{298.15}$), of the gas reactants on CoN_3-G and CoN_4-G. All energies are in eV.

Complex	E_{ads} (eV)	$q_{Co/ads}$(e)	$\Delta H_{298.15}$ (eV)	$\Delta G_{298.15}$ (eV)
CoN₃-G	-	+0.46	-	-
A	-0.38	+0.33/+0.14	-0.34	-0.02
B	-1.24	+0.71/-0.46	-1.22	-0.72
C	-0.02	+0.72/-0.51	0.01	0.36
O-CoN₃-G	-2.93	+0.80/-0.52	-2.86	-2.48
CoN₄-G	-	+0.74	-	-
D	-0.21	+0.68/+0.07	-0.16	0.11
E	-0.24	+0.72/+0.04	-0.20	0.16

The O_2 molecule adopts an end-on configuration on CoN_4-G at a distance of O-Co = 1.95 Å. it adsorbs weakly on the CoN_4-G surface with a low adsorption energy E_{ads} = -0.24 eV, which can be due to the stronger binding energy of Co-N (-7.81 eV) (see Table 1). The obtained adsorption energy value is somewhat lower than the value reported by Feng et al. (E_{ads} = -0.85 eV) [101], FeN_4-G (E_{ads} = -0.98 eV) and MnN_4-G (E_{ads} = -0.35 eV) [102, 103]. Consistent with the weak interaction, a negligible charge of +0.04 e is transferred from the surface to the adsorbed O_2 molecule. In the EDD map, the blue color areas around the Co-O bond confirm the weak interaction of O_2 with the surface. However, the formation of complex E is exothermic $\Delta H_{298.15}$ = -0.20 eV and endergonic $\Delta G_{298.15}$ = 0.16 eV.

Since the interaction of O_2 with CoN_3-G is stronger than that on CoN_4-G, we also evaluated the dissociation of O_2 on CoN_3-G to confirm the stability of the adsorbed structure toward oxygen dissociation. To find the energy profile of the O_2 decomposition, we started with the most stable adsorption configuration of O_2 on CoN_3-G (complex B) as IS and shown in Figure S4. Passing via the TS structure, the final state (FS) is obtained in which two individual O atoms are dissociatively adsorbed on Co and C atom of the surface. The formed O-Co and O-C bond lengths are 1.62 Å and 1.37 Å, respectively. The calculated activation barrier for the O_2 dissociation on CoN_3-G is calculated to be E_{act} = 2.76 eV and the reaction is endothermic, $\Delta H_{298.15}$ = 1.23 eV, and endergonic $\Delta G_{298.15}$ = 1.20 eV. The large decomposition barrier of O_2 on CoN_3-G confirms the stability of the adsorbed O_2 molecule over the surface and its low tendency to dissociate over the CoN_3-G surface.

According to above discussions and previous investigations [100, 104], we conclude that amongst the studied substrates, CoN_3-G is more active toward adsorption of gas reactants, especially O_2 molecule, and therefore is more favourable for methane conversion reaction which is in good agreement with Kattel et al. work [29]. The higher adsorption energy of O_2 molecule than methane reveals that the reactive Co sites will be dominantly covered by the O_2 when exposed to a CH_4/O_2 mixture as the reaction gas. However, the co-adsorption of CH_4 and O_2 on CoN_3-G (E_{ads} = -1.66 eV) is

stronger than the sum of the individual adsorption of CH_4 or O_2 on CoN_3-G (see Table 2). Therefore, we propose that all the reaction pathways start with the co-adsorption configuration of CH_4 and O_2 on the surface.

Recent theoretical studies [105-107] reported that the N_2O molecule attaches to metal-embedded nanostructures via different configurations. It may adsorb via a linear parallel position with the surface, a [3+2]- or [2+2]-cycloaddition configuration. Here, on CoN_3-G, the N_2O molecule adsorbs weakly, E_{ads} = -0.02 eV, via its O and N atoms with the Co atom of the surface while the N–N–O angle decreases from 180° in the gas phase to 123.37° in the adsorbed form (configuration C, Figure 2). Interestingly, upon the adsorption of N_2O on the surface, it immediately dissociates to N_2(g) and atomic O^* molecule above active Co site (see Figure S5). The reaction is barrierless and thermodynamically favourable at room temperature ($\Delta H_{298.15}$ = -2.35 eV, $\Delta G_{298.15}$ = -2.43 eV). It is shown that in the final state the atomic O^* adsorbs chemically on Co atom with Co-O bond length of 1.81 Å and E_{ads} = -1.49 eV.

We also studied the effect of the substrate size on the adsorption behaviour of the gas species on CoN_3-G. To achieve this, a larger graphene flake with 110 carbon and 28 hydrogen atoms (with about 1.5 times larger surface area) is considered as pure graphene flake. All the configurations are optimized using different spin multiplicities, singlet, doublet, triplet, and quadruplet. Amongst those configurations, the energetically more favourable configurations have been chosen as the main structures. The calculated adsorption energy of the Co atom into the pyridinic-N_3 graphene flake along with the adsorption energies of the gas reactants on CoN_3-G are listed in Table S4.

Our results show that by increasing the size of the graphene flake the geometry of the structures do not change while the adsorption energy of O_2, CH_4, and N_2O increases by almost 50%, 3.3%, and 36%, respectively. Nevertheless, we also find that in spite of this increase in adsorption energy, increasing the size of the graphene flake has no significant effect on the general concepts of the used catalyst toward the gas reactants. Indeed, we still find that the O_2 molecule pre-adsorbs on the active Co site of the surface while methane physisorbs on the CoN_3-G flake. Moreover, the dissociation of N_2O molecule to $N_2 + O^*$ proceeds via a negligible barrier energy proposing that still the N_2O molecule is the more favourable oxidant for methane oxidation. Since increasing the size of the graphene-flake did not change either the overall adsorption behaviour of the catalyst or even their corresponding charge transfer, to avoid expensive calculations, we continued using the smaller-sized graphene-flake.

3.3 Conversion of methane to methanol on monolayer CoN_3-G

The energy landscapes for CH_x (x=0-4) adsorption and CH_x (x=1-4) dehydrogenation over CoN_3-G along with the most probable C-C coupling reaction are explained and shown in the Supporting information. There are two different mechanisms for C-H bond cleavage, a surface-stabilized or a radical-like mechanism [78, 108]. In the first mechanism, the carbon atom of methane molecule partially interacts with the catalyst, while in the radical-like mechanism there is no binding or interaction with the catalyst. It is known that the radical-like pathway is the more probable route for single-atom catalysts [109] due to the lower concentrations of the active sites on these substrates making them promising candidates for direct methane to methanol oxidation [110]. We propose two different pathways for the direct conversion of CH_4 to CH_3OH on CoN_3-G using N_2O and O_2 as an oxidant. N_2O acts as an O-donor compound that provides atomic oxygen to oxidize methane to methanol. Depending on the oxidation agent, the formed intermediates, and subsequently, the reaction pathways are different. The formed intermediates are a combination of $^*OH$, CH_3^*, $^*OOH$, and CH_3O^*. The schematic reaction mechanisms of oxidation routes are shown in Scheme 1. Most of the reactions

proceed via the LH mechanism.

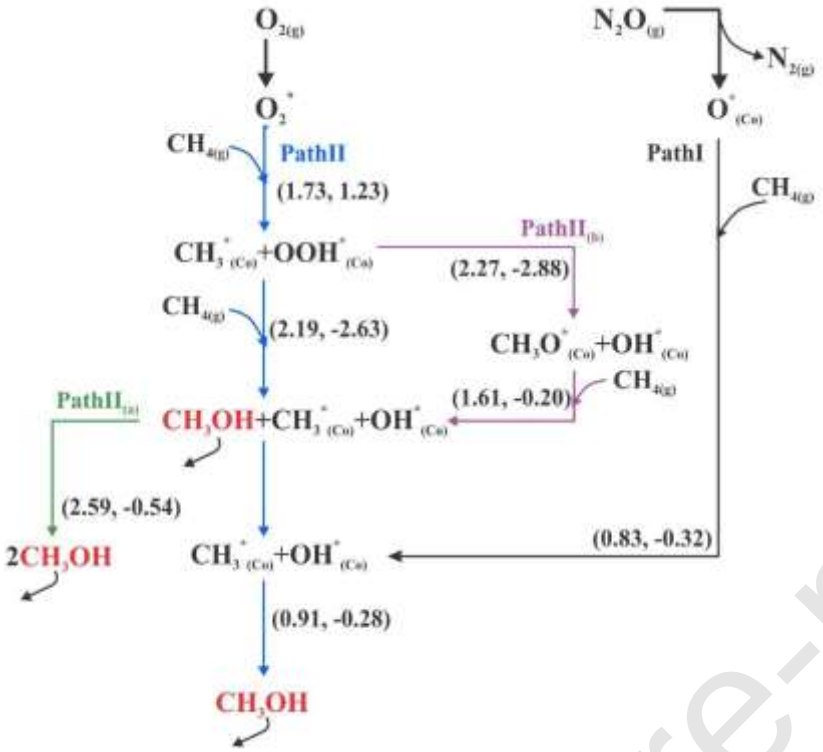

Scheme 1. Proposed reaction pathways on CoN_3-G. The values in parentheses refer to the energy barriers and enthalpy of the reaction. All the energy values are in eV

3.3.1 Methane to methanol oxidation by N_2O

Upon desorption of N_2, the remained atomic oxygen reacts with methane to form methanol. This pathway goes through the formation of CH_3^* and OH^* intermediate species. The related stationary structures along with the preferential potential energy pathways are shown in Figure 3. The calculated reaction heats and the corresponding barriers are summarized in Table 3.

In pathway I, the oxidation reaction starts with co-adsorption of O^* and CH_4 named as IS-1. Hydrogen abstraction with oxygen occurs passing via a low energy barrier of E_{act} = 0.83 eV results in the formation of CH_3^* and $^*OH$ intermediate species on top of the Co site (MS-1) that is in good agreement with Yuan et al. work (E_{act} = 0.7 eV) [106]. Then, the combination of CH_3^* and $^*OH$ species produces the methanol molecule on CoN_3-G surface. The required energy barrier of this reaction is E_{act} = 0.91 eV. According to the thermodynamic results, all the reactions are exothermic and exergonic (see Table 3). Due to the higher activation energy of the reaction MS-1⟶ P-1, we propose it to be the rate-limiting step.

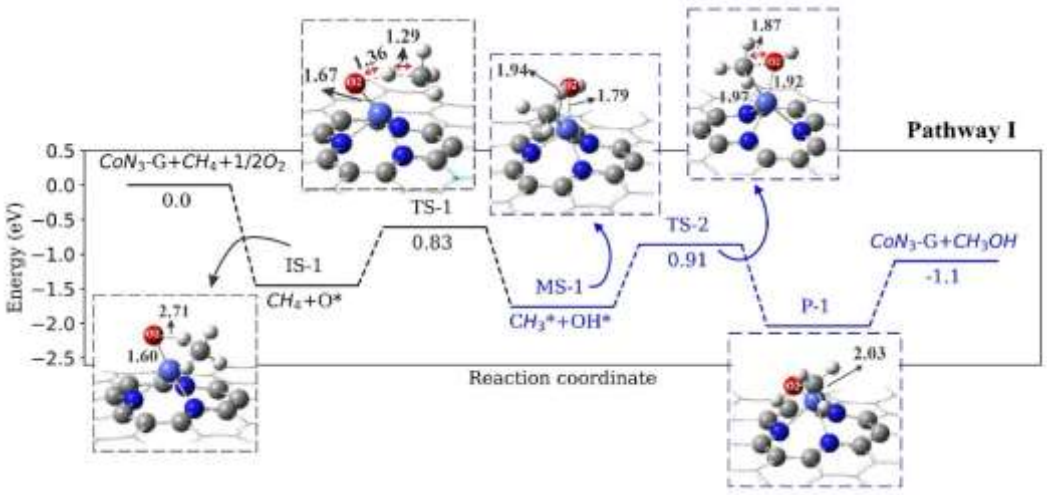

Figure 3. The optimized stationary points for the methane oxidation on CoN_3-G along with the corresponding energy profile of methane conversion by N_2O. All distances are in Å

Table 3. The calculated forward and backward energy barrier (E_{act-f}, E_{act-b}), change of enthalpy ($\Delta H_{298.15}$), and change of Gibbs free energy ($\Delta G_{298.15}$) of the proposed pathway I for methane oxidation reaction on CoN_3-G.

Reaction	E_{act-f} (eV)	E_{act-b} (eV)	ΔH_{298} (eV)	ΔG_{298} (eV)
Pathway I				
$N_2O(g) \longrightarrow N_2(g) + O^*$	0.00	2.27	-2.35	-2.43
$CH_4(g) + O^* \longrightarrow CH_3^* + OH^*$	0.83	1.15	-0.32	-0.30
$CH_3^* + OH^* \longrightarrow CH_3OH(g) + {}^*$	0.91	1.19	-0.28	-0.28

3.3.2 Methane to methanol oxidation by O_2

The proposed pathway II starts with the coadsorption of O_2 and CH_4 at a distance of H-O2 = 2.40 Å above the surface (Figure 4, IS-2). Interestingly, we found that the C-H and Co-O cleavage of methane and adsorbed atomic O^* has the highest barrier energies of E_{act} = 1.73 eV and E_{act} = 2.19 eV, respectively, which inhibited the formation of methanol. In both first and second reaction of methane with oxygen, breaking of the C−H bond occurs concurrently with the formation of an O-H bond and Co-C bond on CoN_3-G, and a further elongation of the O−O bond to 1.97 Å. The formation of the first CH_3OH occurs with the introduction of the second methane to the system through reaction IS-3⟶P-2. Although the activation of the second CH_4 requires ~0.46 eV more energy, it is more exergonic (see Table 4). The second CH_3OH is formed upon the association of the CH_3^* and $^*OH$ species with a reasonable energy barrier of 0.91 eV. Finally, upon the desorption of the second CH_3OH, E_{des}= 0.57 eV, the catalytic cycle is closed. As CH_4 is only physisorbed at Co active site and then reacts with preadsorbed O_2, the methane conversion mechanism in all the reactions can be described as an ER mechanism, except the reaction MS-1⟶ P-1 that proceeds via the LH mechanism. The rate-limiting step is the formation of P-2 which is related to the second C-H and Co-O bond cleavage.

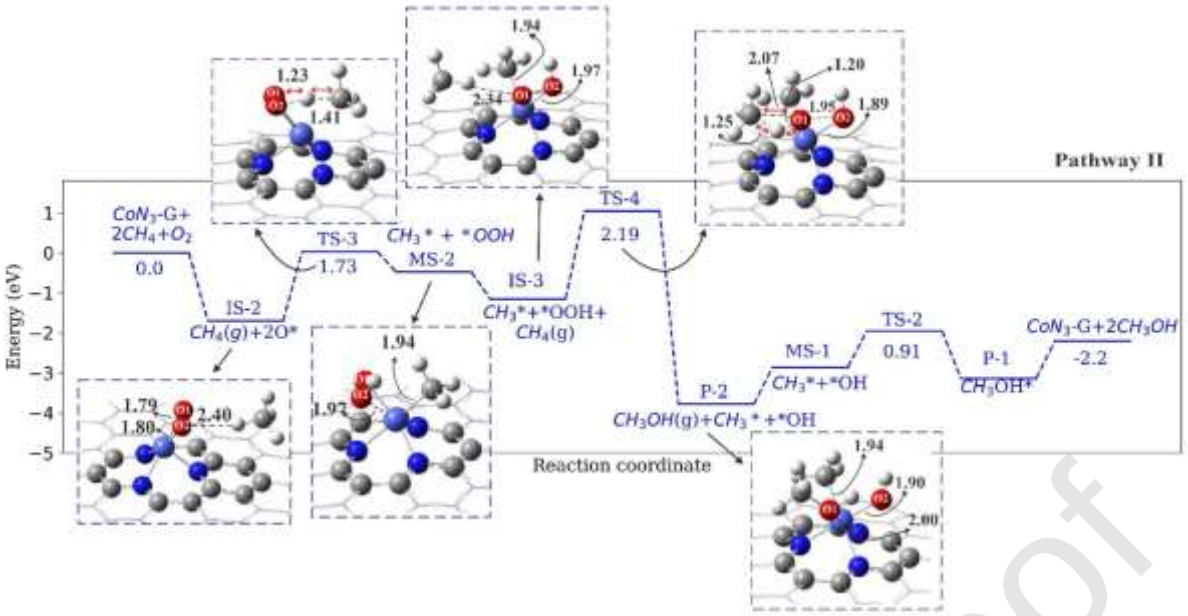

Figure 4. The optimized stationary points for methane oxidation on CoN_3-G along with the corresponding potential energy profile of pathway II. All distances are in Å

We also investigated the other possibilities of methanol formation on CoN_3-G by the formation of other intermediates. We found two other possible pathways (labeled as pathways $II_{(a)}$ and $II_{(b)}$) that goes via the formation and recombination of CH_3^*, O^*, OH^*, and CH_3O^* species on CoN_3-G. The related potential energy profile is shown in Figure S8. The calculated activation energies and thermodynamic values are listed in Table 4. One can see from Figure S8 that in Pathway $II_{(a)}$ and $II_{(b)}$ the reaction MS-2 ⟶ MS-3 (formation of CH_3O^* and $^*OH$) and P-2 ⟶ P-3 requires high energy barrier of E_{act}= 2.27 eV and E_{act}= 2.59 eV, respectively. Therefore, we estimate that the possibility of methane conversion to methanol via pathways $II_{(a)}$ and $II_{(b)}$ is very low.

Table 4. The calculated energy barrier (E_{act}), change of enthalpy ($\Delta H_{298.15}$), and change of Gibbs free energy ($\Delta G_{298.15}$) for the proposed pathways II, $II_{(a)}$, and $II_{(b)}$ for methane oxidation reaction on CoN_3-G.

Reaction	E_{act} (eV)	$\Delta H_{298.15}$ (eV)	$\Delta G_{298.15}$ (eV)
Pathway II			
$O_2(g) + {}^* \longrightarrow 2O^*$	0.00	-1.22	-0.72
$CH_4(g) + 2O^* \longrightarrow CH_3^* + {}^*OOH$	1.73	1.23	1.38
$CH_4(g) + CH_3^* + {}^*OOH \longrightarrow CH_3OH(g) + CH_3^* + {}^*OH$	2.19	-2.63	-2.52
$CH_3^* + {}^*OH \longrightarrow CH_3OH(g) + {}^*$	0.91	-0.28	-0.28
Pathways $II_{(a)}$ and $II_{(b)}$			
$CH_3^* + {}^*OOH \longrightarrow CH_3O^* + {}^*OH$	2.27	-2.88	-2.97
$CH_4(g) + CH_3O^* + {}^*OH \longrightarrow CH_3OH(g) + CH_3^* + {}^*OH$	1.61	-0.20	-0.20
$CH_3OH(g) + CH_3^* + {}^*OH \longrightarrow 2CH_3OH(g) + {}^*$	2.59	-0.54	-0.47

In fact, to produce methanol, the most favourable pathway is pathway I, in which methane oxidation reaction is catalyzed by atomic oxygen, which is donated to the system by dissociative adsorption of N_2O over CoN_3-G. It proceeds via the LH mechanism and all the reactions are thermodynamically favourable. Therefore, we propose that CoN_3-G can actively convert methane to methanol using N_2O as an oxidant agent thanks to the lower activation barriers.

One of the greatest challenges in the catalysts which are used for methane oxidation to methanol is that they can even better cleave the O-H bond of the formed methanol which leads to its overoxidation to CO_2 and H_2O. Thus, we tested the activity of CoN_3-G toward the over-oxidation of methanol. Since

the investigation of the complete over-oxidation process is not the main focus of this paper, only the primary reactions of methanol over-oxidation to CO_2 and H_2O on CoN_3-G were calculated. Our results reveal that methanol oxidation goes through two different routes: (i) O-H bond cleavage, reaction IS-5→MS-4 (ii) C-H bond cleavage IS-5→MS-5 (see Figure 5). We found that the over-oxidation of methanol via reaction pathway IS-5→MS-4 is more probable to proceed than reaction IS-5→MS-5. In IS-5 the methanol molecule adsorbs on Co atom of CoN_3-G with adsorption energy of E_{ads}= -1.77 eV. The H abstraction by introduced atomic oxygen to the system occurs via the cleavage of the O-H bond with a low energy barrier of E_{act} = 0.23 eV. This reaction is exothermic and exergonic ($\Delta H_{298.15}$ = -0.25 eV, $\Delta G_{298.15}$ = -0.23 eV). In the next step, H is abstracted from the C atom via TS-9 to form H_2O while H_2CO adsorbs over CoN_3-G with Co-O bond length of 1.31 Å (see Figure 5, P-4) and energy barrier of E_{act} = 0.56 eV.

In pathway (ii), the C-H bond cleavage requires overcoming a higher energy barrier, E_{act} = 1.29 eV, than that of O-H cleavage. In addition, the corresponding reaction is not thermodynamically favourable at ambient conditions ($\Delta H_{298.15}$ = 0.57 eV, $\Delta G_{298.15}$ = 0.51 eV). These initial calculations for the probability of methanol over-oxidation indicate that although CoN_3-G could better catalyze methane conversion to methanol, it might also oxidize the produced methanol molecule to CO_2 and H_2O or other intermediates with low activation barriers. In practice, this can affect the conversion percentage of methane to methanol.

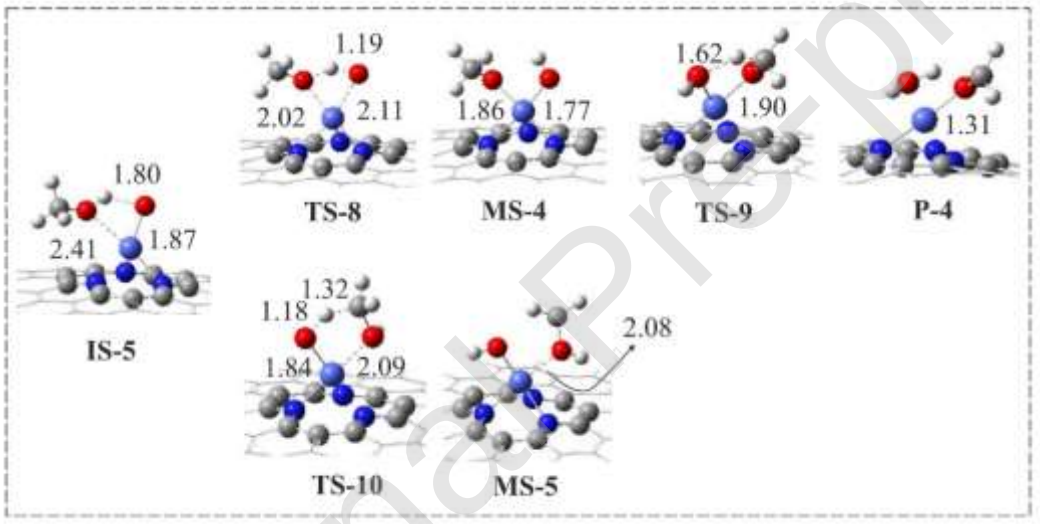

Figure 5. The optimized stationary points for methanol over-oxidation on CoN_3-G. All distances are in Å

4 Conclusions

In summary, the geometric stability and catalytic activity of Co-SV-G, Co-dV-G, CoN_3-G, and CoN_4-G toward adsorption of gas reactants are studied in detail employing DFT calculations. Studying the geometric, electronic, and thermodynamic properties of all optimized structures showed that amongst other modified graphene flakes, CoN_3-G and CoN_4-G are energetically more stable than other substrates. Investigating the adsorption behavior of CoN_3-G and CoN_4-G toward the gas reactants indicated that CoN_3-G has a higher tendency for the adsorption of methane and oxygen. Therefore, we chose CoN_3-G as for methane-to-methanol oxidation. Two powerful oxidants are used for catalyzing methane oxidation, viz. O_2 and N_2O. N_2O adsorbs dissociatively on CoN_3-G providing atomic oxygen for methane oxidation. Oxidation of methane using N_2O proceeds via two steps on CoN_3-G with considerably lower energy barriers while using O_2 as oxidant proceeds through a pathway with higher activation barriers. All the C-H bond cleavage reactions proceed through the ER mechanism and

followed by the LH mechanism.

One of the greatest challenges in methane oxidation processes is the over-oxidation of methanol to CO_2 and H_2O or other intermediates. According to our calculations, the dominant pathway for methanol over-oxidation on CoN_3-G occurs through two main routes, viz. the O-H bond cleavage route with low energy barriers of E_{act} = 0.23 eV and E_{act} = 0.56 eV, and the C-H bond cleavage route with a higher barrier of E_{act} = 1.29 eV. Thus, we propose that CoN_3-G might be a good catalyst for methane conversion but it can also catalyze the oxidation of methanol to CO_2 and H_2O or other intermediates due to the required low activation barriers. In practice, this can affect the conversion percentage of methane to methanol.

Investigating the adsorption (CH_x, x=0-4) and dehydrogenation (CH_x, x=1-4) process of methane on CoN_3-G indicated that the adsorption energy of CH_4, CH_3, CH_2, CH, and C on CoN_3-G increases by reducing the number of hydrogen atoms. In the dehydrogenation process, all pathways start from the C-H scission ($CH_x \longrightarrow CH_{x-1} + H$) and dehydrogenation of methane to methyl showed the lower energy barrier of 1.10 eV. This makes the C-C coupling of the two-methyl group to ethane easier passing via an energy barrier of 0.45 eV. To the best of our knowledge, this is the first report on the direct oxidation of methane-to-methanol on CoN_3-G using different oxidants. We believe our findings may open a new way to design such heteroatom doped graphene-based single-atom catalysts to eliminate toxic molecules, which are harmful to the environment.

Credit Author statement

Parisa Nematollahi: Investigation, calculations, methodology, analyzing the data, writing, original draft preparation, problem solving, visualization: plotting and designing the Figures, reviewing and editing.
Erik Neyts: Reviewing and editing.

5 Conflicts of interest

There are no conflicts to declare.

6 Acknowledgments

This work was performed with the financial support from the Doctoral Fund of the Antwerp University (NO. BOFLP33099). All the simulations are performed on resources provided by the high-performance computing center of Antwerp University.

References

[1] V.L. Sushkevich, D. Palagin, M. Ranocchiari, J.A. van Bokhoven, Selective anaerobic oxidation of methane enables direct synthesis of methanol, Science, 356 (2017) 523-527.
[2] B. Wang, S. Albarracín-Suazo, Y. Pagán-Torres, E. Nikolla, Advances in methane conversion processes, Catal. Today, 285 (2017) 147-158.
[3] D. Pakhare, J. Spivey, A review of dry (CO_2) reforming of methane over noble metal catalysts, Chem. Soc. Rev., 43 (2014) 7813-7837.
[4] J. Bitter, K. Seshan, J. Lercher, Mono and bifunctional pathways of CO_2/CH_4 reforming over Pt and Rh based catalysts, J. Catal., 176 (1998) 93-101.
[5] Y.-Z. Lin, J. Sun, J. Yi, J.-D. Lin, H.-B. Chen, D.-W. Liao, Energetics of chemisorption and conversion of methane on transition metal surfaces, J mol. Struc-THEOCHEM, 587 (2002) 63-71.
[6] C. Carrara, J. Munera, E. Lombardo, L. Cornaglia, Kinetic and stability studies of Ru/La_2O_3 used in the dry reforming of methane, Top. Catal., 51 (2008) 98-106.
[7] K. Sutthiumporn, S. Kawi, Promotional effect of alkaline earth over $Ni–La_2O_3$ catalyst for CO_2 reforming of CH4: role of surface oxygen species on H_2 production and carbon suppression, Int. J. Hydrogen Energ., 36 (2011) 14435-14446.
[8] Z. Bian, S. Das, M.H. Wai, P. Hongmanorom, S. Kawi, A Review on Bimetallic Nickel-Based Catalysts for CO_2 Reforming of Methane, ChemPhysChem, 18 (2017) 3117-3134.
[9] J. Liu, B.R. Bunes, L. Zang, C. Wang, Supported single-atom catalysts: synthesis, characterization, properties, and applications, Environ. Chem. Lett., 16 (2018) 477-505.
[10] H. Wang, Q. Wang, Y. Cheng, K. Li, Y. Yao, Q. Zhang, C. Dong, P. Wang, U. Schwingenschlögl, W. Yang, Doping monolayer graphene with single-atom substitutions, Nano Lett., 12 (2011) 141-144.
[11] K. Jiang, S. Back, A.J. Akey, C. Xia, Y. Hu, W. Liang, D. Schaak, E. Stavitski, J.K. Nørskov, S. Siahrostami, Highly selective oxygen reduction to hydrogen peroxide on transition metal single-atom coordination, Nat. Commun., 10 (2019) 1-11.
[12] D.-W. Wang, D. Su, Heterogeneous nanocarbon materials for oxygen reduction reaction, Energy Environ. Sci., 7 (2014) 576-591.
[13] B. Guo, L. Fang, B. Zhang, J.R. Gong, Graphene Doping: A Review, Insciences J., (2011) 80-89.
[14] G. Kyriakou, M.B. Boucher, A.D. Jewell, E.A. Lewis, T.J. Lawton, A.E. Baber, H.L. Tierney, M. Flytzani-Stephanopoulos, E.C.H. Sykes, Isolated metal atom geometries as a strategy for selective heterogeneous hydrogenations, Science, 335 (2012) 1209-1212.
[15] M. Moses-DeBusk, M. Yoon, L.F. Allard, D.R. Mullins, Z. Wu, X. Yang, G. Veith, G.M. Stocks, C.K. Narula, CO oxidation on supported single Pt atoms: Experimental and ab initio density functional studies of CO interaction with Pt atom on θ-Al_2O_3 (010) surface, J. Am. Chem. Soc., 135 (2013) 12634-12645.
[16] R. Li, Z. Wei, X. Gou, W. Xu, Phosphorus-doped graphene nanosheets as efficient metal-free oxygen reduction electrocatalysts, RSC Adv., 3 (2013) 9978-9984.
[17] M.D. Esrafili, N. Saeidi, P. Nematollahi, Si-doped graphene: A promising metal-free catalyst for oxidation of SO 2, Chem. Phys. Lett., 649 (2016) 37-43.
[18] Y. Chen, X.-c. Yang, Y.-j. Liu, J.-x. Zhao, Q.-h. Cai, X.-z. Wang, Can Si-doped graphene activate or dissociate O_2 molecule? J. Mol. Graph. Model., 39 (2013) 126-132.
[19] Y. Li, Z. Zhou, G. Yu, W. Chen, Z. Chen, CO catalytic oxidation on iron-embedded graphene: computational quest for low-cost nanocatalysts, J. Phys. Chem. C., 114 (2010) 6250-6254.
[20] D. Cortés-Arriagada, N. Villegas-Escobar, A DFT analysis of the adsorption of nitrogen oxides on Fe-doped graphene, and the electric field induced desorption, Appl. Surf. Sci., 420 (2017) 446-455.
[21] Y. Tong, Y. Wang, Q. Wang, Theoretical investigation for the reaction of N_2O with CO catalyzed by Pt-Graphene, Struct. Chem., (2017).
[22] S. Sun, G. Zhang, N. Gauquelin, N. Chen, J. Zhou, S. Yang, W. Chen, X. Meng, D. Geng, M.N. Banis, Single-atom catalysis using Pt/graphene achieved through atomic layer deposition, Sci. Rep., 3 (2013) 1775.
[23] L. Ma, J.-M. Zhang, K.-W. Xu, V. Ji, A first-principles study on gas sensing properties of graphene and Pd-doped graphene, Appl. Surf. Sci., 343 (2015) 121-127.
[24] T.-T. Jia, C.-H. Lu, Y.-F. Zhang, W.-k. Chen, A comparative study of CO catalytic oxidation on Pd-anchored graphene oxide and Pd-embedded vacancy graphene, J. Nanopart. Res., 16 (2014) 1-11.
[25] E.J. Santos, A. Ayuela, S. Fagan, J. Mendes Filho, D. Azevedo, A. Souza Filho, D. Sánchez-Portal, Switching on magnetism in Ni-doped graphene: Density functional calculations, Phys. Rev. B, 78 (2008) 195420.
[26] Y.-g. Wu, M. Wen, Q.-s. Wu, H. Fang, Ni/graphene nanostructure and its electron-enhanced catalytic action for hydrogenation reaction of nitrophenol, J. Phys. Chem. C., 118 (2014) 6307-6313.

[27] Y. Tang, Z. Yang, X. Dai, Trapping of metal atoms in the defects on graphene, J. Chem. Phys., 135 (2011) 224704.
[28] X. Qin, Q. Meng, W. Zhao, Effects of Stone–Wales defect upon adsorption of formaldehyde on graphene sheet with or without Al dopant: a first principle study, Surf. Sci., 605 (2011) 930-933.
[29] S. Kattel, P. Atanassov, B. Kiefer, Stability, electronic and magnetic properties of in-plane defects in graphene: A first-principles study, J. Phys. Chem. C., 116 (2012) 8161-8166.
[30] Z. He, K. He, A.W. Robertson, A.I. Kirkland, D. Kim, J. Ihm, E. Yoon, G.-D. Lee, J.H. Warner, Atomic structure and dynamics of metal dopant pairs in graphene, Nano Lett., 14 (2014) 3766-3772.
[31] S. Kattel, P. Atanassov, B. Kiefer, Density functional theory study of the oxygen reduction reaction mechanism in a BN co-doped graphene electrocatalyst, J. Mater. Chem. A, 2 (2014) 10273-10279.
[32] D. Wei, Y. Liu, Y. Wang, H. Zhang, L. Huang, G. Yu, Synthesis of N-doped graphene by chemical vapor deposition and its electrical properties, Nano Lett., 9 (2009) 1752-1758.
[33] Y.-C. Lin, C.-Y. Lin, P.-W. Chiu, Controllable graphene N-doping with ammonia plasma, Appl. Phys. Lett., 96 (2010).
[34] D. Usachov, O. Vilkov, A. Gruneis, D. Haberer, A. Fedorov, V.K. Adamchuk, A.B. Preobrajenski, P. Dudin, A. Barinov, M. Oehzelt, C. Laubschat, D.V. Vyalikh, Nitrogen-doped graphene: efficient growth, structure, and electronic properties, Nano Lett., 11 (2011) 5401-5407.
[35] Y.J. Cho, H.S. Kim, S.Y. Baik, Y. Myung, C.S. Jung, C.H. Kim, J. Park, H.S. Kang, Selective nitrogen-doping structure of nanosize graphitic layers, J. Phys. Chem. C., 115 (2011) 3737-3744.
[36] Y. Fujimoto, S. Saito, Formation, stabilities, and electronic properties of nitrogen defects in graphene, Phys. Rev. B, 84 (2011) 245446.
[37] R. Lv, Q. Li, A.R. Botello-Méndez, T. Hayashi, B. Wang, A. Berkdemir, Q. Hao, A.L. Elías, R. Cruz-Silva, H.R. Gutiérrez, Nitrogen-doped graphene: beyond single substitution and enhanced molecular sensing, Sci. Rep., 2 (2012) 586.
[38] V.D. Pham, J.r.m. Lagoute, O. Mouhoub, F.d.r. Joucken, V. Repain, C. Chacon, A. Bellec, Y. Girard, S. Rousset, Electronic interaction between nitrogen-doped graphene and porphyrin molecules, ACS Nano, 8 (2014) 9403-9409.
[39] Y. Wang, Y. Shao, D.W. Matson, J. Li, Y. Lin, Nitrogen-doped graphene and its application in electrochemical biosensing, ACS Nano, 4 (2010) 1790-1798.
[40] H. Wang, T. Maiyalagan, X. Wang, Review on recent progress in nitrogen-doped graphene: synthesis, characterization, and its potential applications, ACS Catal., 2 (2012) 781-794.
[41] H. Fei, R. Ye, G. Ye, Y. Gong, Z. Peng, X. Fan, E.L. Samuel, P.M. Ajayan, J.M. Tour, Boron-and nitrogen-doped graphene quantum dots/graphene hybrid nanoplatelets as efficient electrocatalysts for oxygen reduction, ACS Nano, 8 (2014) 10837-10843.
[42] M.D. Esrafili, R. Mohammad- Valipour, S.M. Mousavi- Khoshdel, P. Nematollahi, A Comparative Study of CO Oxidation on Nitrogen- and Phosphorus- Doped Graphene, ChemPhysChem, 16 (2015) 3719-3727.
[43] A.L.M. Reddy, A. Srivastava, S.R. Gowda, H. Gullapalli, M. Dubey, P.M. Ajayan, Synthesis of nitrogen-doped graphene films for lithium battery application, ACS Nano, 4 (2010) 6337-6342.
[44] X. Zhou, L.J. Wan, Y.G. Guo, Binding SnO_2 nanocrystals in nitrogen- doped graphene sheets as anode materials for lithium- ion batteries, Adv. Mater., 25 (2013) 2152-2157.
[45] Y. Zheng, Y. Jiao, Y. Zhu, L.H. Li, Y. Han, Y. Chen, A. Du, M. Jaroniec, S.Z. Qiao, Hydrogen evolution by a metal-free electrocatalyst, Nat. Commun., 5 (2014) 3783.
[46] L. Zhang, Z. Xia, Mechanisms of Oxygen Reduction Reaction on Nitrogen-Doped Graphene for Fuel Cells, J. Phys. Chem. C., 115 (2011) 11170-11176.
[47] H. Liu, Y. Liu, D. Zhu, Chemical doping of graphene, J. Mater. Chem., 21 (2011) 3335-3345.
[48] X. Wang, Y. Liu, D. Zhu, L. Zhang, H. Ma, N. Yao, B. Zhang, Controllable growth, structure, and low field emission of well-aligned CN x nanotubes, J. Phys. Chem. B., 106 (2002) 2186-2190.
[49] X. Zhang, Z. Lu, Z. Yang, The mechanism of oxygen reduction reaction on CoN_4 embedded graphene: A combined kinetic and atomistic thermodynamic study, Int. J. Hydrogen Energ., 41 (2016) 21212-21220.
[50] X. Sun, K. Li, C. Yin, Y. Wang, M. Jiao, F. He, X. Bai, H. Tang, Z. Wu, Dual-site oxygen reduction reaction mechanism on CoN_4 and CoN_2 embedded graphene: Theoretical insights, Carbon, 108 (2016) 541-550.
[51] S. Gupta, D. Tryk, I. Bae, W. Aldred, E. Yeager, Heat-treated polyacrylonitrile-based catalysts for oxygen electroreduction, J. Appl. Electrochem., 19 (1989) 19-27.
[52] C.W. Bezerra, L. Zhang, K. Lee, H. Liu, A.L. Marques, E.P. Marques, H. Wang, J. Zhang, A review of Fe–N/C and Co–N/C catalysts for the oxygen reduction reaction, Electrochim. Acta, 53 (2008) 4937-4951.
[53] B. Guo, Q. Liu, E. Chen, H. Zhu, L. Fang, J.R. Gong, Controllable N-doping of graphene, Nano Lett., 10 (2010) 4975-4980.
[54] H. Fei, Y. Yang, Z. Peng, G. Ruan, Q. Zhong, L. Li, E.L. Samuel, J.M. Tour, Cobalt nanoparticles embedded in nitrogen-doped carbon for the hydrogen evolution reaction, ACS Appl. Mater. Interfaces, 7 (2015) 8083-8087.

[55] Z. Wang, S. Xiao, Z. Zhu, X. Long, X. Zheng, X. Lu, S. Yang, Cobalt-embedded nitrogen doped carbon nanotubes: a bifunctional catalyst for oxygen electrode reactions in a wide pH range, ACS Appl. Mater. Interfaces, 7 (2015) 4048-4055.
[56] J.D. Blakemore, R.H. Crabtree, G.W. Brudvig, Molecular catalysts for water oxidation, Chem. Rev., 115 (2015) 12974-13005.
[57] H. Kim, J. Park, I. Park, K. Jin, S.E. Jerng, S.H. Kim, K.T. Nam, K. Kang, Coordination tuning of cobalt phosphates towards efficient water oxidation catalyst, Nat. Commun., 6 (2015) 8253.
[58] H. Fei, J. Dong, M.J. Arellano-Jiménez, G. Ye, N.D. Kim, E.L. Samuel, Z. Peng, Z. Zhu, F. Qin, J. Bao, Atomic cobalt on nitrogen-doped graphene for hydrogen generation, Nat. Commun., 6 (2015) 8668.
[59] D. Lašič Jurković, H. Puliyalil, A. Pohar, B. Likozar, Plasma- activated methane partial oxidation reaction to oxygenate platform chemicals over Fe, Mo, Pd and zeolite catalysts, Int. J. Energy Res., 43 (2019) 8085-8099.
[60] X. Zou, X. Huang, A. Goswami, R. Silva, B.R. Sathe, E. Mikmeková, T. Asefa, Cobalt- embedded nitrogen- rich carbon nanotubes efficiently catalyze hydrogen evolution reaction at all pH values, Angew. Chem., 53 (2014) 4372-4376.
[61] S. Kattel, G. Wang, A density functional theory study of oxygen reduction reaction on Me–N_4 (Me= Fe, Co, or Ni) clusters between graphitic pores, J. Mater. Chem. A, 1 (2013) 10790-10797.
[62] Y. Zheng, Y. Jiao, J. Chen, J. Liu, J. Liang, A. Du, W. Zhang, Z. Zhu, S.C. Smith, M. Jaroniec, Nanoporous graphitic-C_3N_4@carbon metal-free electrocatalysts for highly efficient oxygen reduction, J. Am. Chem. Soc., 133 (2011) 20116-20119.
[63] S. Kattel, P. Atanassov, B. Kiefer, Catalytic activity of Co-N_x/C electrocatalysts for oxygen reduction reaction: a density functional theory study, Phys. Chem. Chem. Phys., 15 (2013) 148-153.
[64] D. Abergel, V. Apalkov, J. Berashevich, K. Ziegler, T. Chakraborty, Properties of graphene: a theoretical perspective, Adv. Phys., 59 (2010) 261-482.
[65] A.C. Neto, F. Guinea, N.M. Peres, K.S. Novoselov, A.K. Geim, The electronic properties of graphene, Rev. Mod. Phys., 81 (2009) 109.
[66] Y. Son, Nature (London) https://doi. org/10.1038/nature05180 444, 347 (2006), Google Scholar Y. Son, ML Cohen, and SG Louie, Phys. Rev. Lett. https://doi. org/10.1103/PhysRevLett, 97 (2006) 216803.
[67] H. Zheng, W. Duley, First-principles study of edge chemical modifications in graphene nanodots, Phys. Rev. B, 78 (2008) 045421.
[68] V.D. Dasireddy, D. Hanzel, K. Bharuth-Ram, B. Likozar, The effect of oxidant species on direct, non-syngas conversion of methane to methanol over an $FePO_4$ catalyst material, RSC Adv., 9 (2019) 30989-31003.
[69] P. Nematollahi, E.C. Neyts, Direct methane conversion to methanol on M and MN_4 embedded graphene (M= Ni and Si): A comparative DFT study, Appl. Surf. Sci., 496 (2019) 143618.
[70] M. Frisch, G. Trucks, H. Schlegel, G. Scuseria, M. Robb, J. Cheeseman, G. Scalmani, V. Barone, G. Petersson, H. Nakatsuji, Gaussian 16 Revision A. 03; 2016, There is no corresponding record for this reference.
[71] Y. Zhao, N.E. Schultz, D. Truhlar, Exchange-correlation functional with broad accuracy for metallic and nonmetallic compounds, kinetics, and noncovalent interactions, AIP, 2005.
[72] P. Hay, RJ Chem. Phys. 1985, 82, 270. (b) Wadt, WR; Hay, PJ J. Chem. Phys, 82 (1985) 284.
[73] T. Lu, F. Chen, Multiwfn: a multifunctional wavefunction analyzer, J. Comput. Chem., 33 (2012) 580-592.
[74] Z. Gao, Y. Sun, M. Li, W. Yang, X. Ding, Adsorption sensitivity of Fe decorated different graphene supports toward toxic gas molecules (CO and NO), Appl. Surf. Sci., (2018).
[75] J.W. Ochterski, Thermochemistry in gaussian, Gaussian Inc, (2000) 1-19.
[76] C. Gonzalez, H.B. Schlegel, Improved algorithms for reaction path following: higher- order implicit algorithms, J. Chem. Phys., 95 (1991) 5853-5860.
[77] J.A. Montgomery Jr, M.J. Frisch, J.W. Ochterski, G.A. Petersson, A complete basis set model chemistry. VI. Use of density functional geometries and frequencies, J. Chem. Phys., 110 (1999) 2822-2827.
[78] A.A. Latimer, H. Aljama, A. Kakekhani, J.S. Yoo, A. Kulkarni, C. Tsai, M. Garcia-Melchor, F. Abild-Pedersen, J.K. Nørskov, Mechanistic insights into heterogeneous methane activation, Phys. Chem. Chem. Phys., 19 (2017) 3575-3581.
[79] X. Zhang, Z. Yang, Z. Lu, W. Wang, Bifunctional CoN_x embedded graphene electrocatalysts for OER and ORR: A theoretical evaluation, Carbon, (2018).
[80] F. Gao, G.-L. Zhao, Z. Wang, D. Bagayoko, D.-J. Liu, Catalytic reaction on FeN_4/C site of nitrogen functionalized carbon nanotubes as cathode catalyst for hydrogen fuel cells, Catal. Commun., 62 (2015) 79-82.
[81] W. Orellana, Catalytic properties of transition metal–N_4 moieties in graphene for the oxygen reduction reaction: evidence of spin-dependent mechanisms, J. Phys. Chem. C., 117 (2013) 9812-9818.
[82] D.R. Cooper, B. D'Anjou, N. Ghattamaneni, B. Harack, M. Hilke, A. Horth, N. Majlis, M. Massicotte, L. Vandsburger, E. Whiteway, Experimental review of graphene, ISRN Condensed Matter Physics, (2012).
[83] H. Shin, S. Kang, J. Koo, H. Lee, J. Kim, Y. Kwon, Cohesion energetics of carbon allotropes: Quantum Monte Carlo study, J. Chem. Phys., 140 (2014) 114702.

[84] R. Zacharia, H. Ulbricht, T. Hertel, Interlayer cohesive energy of graphite from thermal desorption of polyaromatic hydrocarbons, Phys. Rev. B, 69 (2004) 155406.
[85] S. Lebègue, J. Harl, T. Gould, J. Ángyán, G. Kresse, J. Dobson, Cohesive properties and asymptotics of the dispersion interaction in graphite by the random phase approximation, Phys. Rev. Lett., 105 (2010) 196401.
[86] N.K. Jaiswal, P. Srivastava, First principles calculations of cobalt doped zigzag graphene nanoribbons, Solid State Commun., 152 (2012) 1489-1492.
[87] E.J. Santos, D. Sánchez-Portal, A. Ayuela, Magnetism of substitutional Co impurities in graphene: realization of single π vacancies, Phys. Rev. B, 81 (2010) 125433.
[88] L. Tsetseris, B. Wang, S. Pantelides, Substitutional doping of graphene: the role of carbon divacancies, Phys. Rev. B, 89 (2014) 035411.
[89] G. Xu, R. Wang, F. Yang, D. Ma, Z. Yang, Z. Lu, CO oxidation on single Pd atom embedded defect-graphene via a new termolecular Eley-Rideal mechanism, Carbon, 118 (2017) 35-42.
[90] F. Banhart, J. Kotakoski, A.V. Krasheninnikov, Structural defects in graphene, ACS Nano, 5 (2010) 26-41.
[91] M. Wang, Z. Wang, Single Ni atom incorporated with pyridinic nitrogen graphene as an efficient catalyst for CO oxidation: first-principles investigation, RSC Adv., 7 (2017) 48819-48824.
[92] M.D. Esrafili, S. Asadollahi, Exploring different reaction mechanisms for oxidation of CO over a single Pd atom incorporated nitrogen-doped graphene: A DFT study, Appl. Surf. Sci., 463 (2019) 526-534.
[93] X. Zhang, Z. Lu, Z. Yang, Single non-noble-metal cobalt atom stabilized by pyridinic vacancy graphene: An efficient catalyst for CO oxidation, Journal of Molecular Catalysis A: Chemical, 417 (2016) 28-35.
[94] F. Li, H. Shu, C. Hu, Z. Shi, X. Liu, P. Liang, X. Chen, Atomic mechanism of electrocatalytically active Co–N complexes in graphene basal plane for oxygen reduction reaction, ACS Appl. Mater. Interfaces, 7 (2015) 27405-27413.
[95] W. Wong, W.R.W. Daud, A.B. Mohamad, A.A.H. Kadhum, K.S. Loh, E. Majlan, Recent progress in nitrogen-doped carbon and its composites as electrocatalysts for fuel cell applications, Int. J. Hydrogen Energ., 38 (2013) 9370-9386.
[96] K. Niu, B. Yang, J. Cui, J. Jin, X. Fu, Q. Zhao, J. Zhang, Graphene-based non-noble-metal Co/N/C catalyst for oxygen reduction reaction in alkaline solution, J. Power Sources, 243 (2013) 65-71.
[97] V.B. Parambhath, R. Nagar, S. Ramaprabhu, Effect of nitrogen doping on hydrogen storage capacity of palladium decorated graphene, Langmuir, 28 (2012) 7826-7833.
[98] D.H. Lee, W.J. Lee, W.J. Lee, S.O. Kim, Y.-H. Kim, Theory, synthesis, and oxygen reduction catalysis of Fe-porphyrin-like carbon nanotube, Phys. Rev. Lett., 106 (2011) 175502.
[99] J. Zhang, Z. Wang, Z. Zhu, The inherent kinetic electrochemical reduction of oxygen into H_2O on FeN_4-carbon: a density functional theory study, J. Power Sources, 255 (2014) 65-69.
[100] X. Liu, Y. Sui, T. Duan, C. Meng, Y. Han, Monodisperse Pt atoms anchored on N-doped graphene as efficient catalysts for CO oxidation: a first-principles investigation, Catal. Sci. Technol, 5 (2015) 1658-1667.
[101] Y. Feng, F. Li, Z. Hu, X. Luo, L. Zhang, X.-F. Zhou, H.-T. Wang, J.-J. Xu, E. Wang, Tuning the catalytic property of nitrogen-doped graphene for cathode oxygen reduction reaction, Phys. Rev. B, 85 (2012) 155454.
[102] S. Kattel, G. Wang, Reaction pathway for oxygen reduction on FeN4 embedded graphene, J. Phys. Chem. Lett., 5 (2014) 452-456.
[103] Z. Lu, G. Xu, C. He, T. Wang, L. Yang, Z. Yang, D. Ma, Novel catalytic activity for oxygen reduction reaction on MnN4 embedded graphene: A dispersion-corrected density functional theory study, Carbon, 84 (2015) 500-508.
[104] L. Panchakarla, K. Subrahmanyam, S. Saha, A. Govindaraj, H. Krishnamurthy, U. Waghmare, C. Rao, Synthesis, structure, and properties of boron- and nitrogen- doped graphene, Adv. Mater., 21 (2009) 4726-4730.
[105] P. Nematollahi, M.D. Esrafili, A DFT study on the N_2O reduction by CO molecule over silicon carbide nanotubes and nanosheets, RSC Adv., 6 (2016) 59091-59099.
[106] J. Yuan, W. Zhang, X. Li, J. Yang, A high performance catalyst for methane conversion to methanol: graphene supported single-atom Co, ChemComm, 54 (2018) 2284-2287.
[107] A. Junkaew, S. Namuangruk, P. Maitarad, M. Ehara, Silicon-coordinated nitrogen-doped graphene as a promising metal-free catalyst for N_2O reduction by CO: a theoretical study, RSC Adv., 8 (2018) 22322-22330.
[108] J.C. Da Silva, R.C. Pennifold, J.N. Harvey, W.R. Rocha, A radical rebound mechanism for the methane oxidation reaction promoted by the dicopper center of a pMMO enzyme: a computational perspective, Dalton Trans., 45 (2016) 2492-2504.
[109] A.A. Latimer, A.R. Kulkarni, H. Aljama, J.H. Montoya, J.S. Yoo, C. Tsai, F. Abild-Pedersen, F. Studt, J.K. Nørskov, Understanding trends in C–H bond activation in heterogeneous catalysis, Nat. Mater., 16 (2017) 225.
[110] C. Hammond, M.M. Forde, M.H. Ab Rahim, A. Thetford, Q. He, R.L. Jenkins, N. Dimitratos, J.A. Lopez- Sanchez, N.F. Dummer, D.M. Murphy, Direct catalytic conversion of methane to methanol in an aqueous medium by using copper- promoted Fe- ZSM- 5, Angew. Chem., 51 (2012) 5129-5133.